

Exploring Chemistry in Microcompartments Using Guided Droplet Collisions in a Branched Quadrupole Trap Coupled to a Single Droplet, Paper Spray Mass Spectrometer

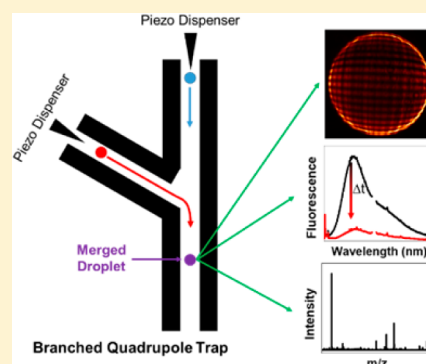
Michael I. Jacobs,^{†,‡,§} James F. Davies,[‡] Lance Lee,^{‡,§} Ryan D. Davis,^{‡,§} Frances Houle,^{‡,§} and Kevin R. Wilson^{*,‡,§}

[†]Department of Chemistry, University of California, Berkeley, California 94720, United States

[‡]Chemical Sciences Division, Lawrence Berkeley National Laboratory, Berkeley, California 94720, United States

Supporting Information

ABSTRACT: Recent studies suggest that reactions in aqueous microcompartments can occur at significantly different rates than those in the bulk. Most studies have used electrospray to generate a polydisperse source of highly charged microdroplets, leading to multiple confounding factors potentially influencing reaction rates (e.g., evaporation, charge, and size). Thus, the underlying mechanism for the observed enhancement remains unclear. We present a new type of electrodynamic balance—the branched quadrupole trap (BQT)—which can be used to study reactions in microdroplets in a controlled environment. The BQT allows for condensed phase chemical reactions to be initiated by colliding droplets with different reactants and levitating the merged droplet indefinitely. The performance of the BQT is characterized in several ways. Sub-millisecond mixing times as fast as $\sim 400 \mu\text{s}$ are measured for low velocity ($\sim 0.1 \text{ m/s}$) collisions of droplets with $< 40 \mu\text{m}$ diameters. The reaction of *o*-phthalaldehyde (OPA) with alanine in the presence of dithiothreitol is measured using both fluorescence spectroscopy and single droplet paper spray mass spectrometry. The bimolecular rate constant for reaction of alanine with OPA is found to be 84 ± 10 and $67 \pm 6 \text{ M}^{-1} \text{ s}^{-1}$ in a $30 \mu\text{m}$ radius droplet and bulk solution, respectively, which demonstrates that bimolecular reaction rate coefficients can be quantified using merged microdroplets and that merged droplets can be used to study rate enhancements due to compartmentalization. Products of the reaction of OPA with alanine are detected in single droplets using paper spray mass spectrometry. We demonstrate that single droplets with $< 100 \text{ pg}$ of analyte can easily be studied using single droplet mass spectrometry.



Chemical reactions in micrometer-sized compartments are ubiquitous in nature, occurring in cells, mineral pores, and atmospheric aerosols. Several recent studies suggest that reactions in confined spaces occur at enhanced rates that can be several orders of magnitude faster than those in the bulk.^{1–7} Although the underlying mechanism remains unclear, three main factors are thought to contribute—increased concentrations due to solvent evaporation, surface acidity (i.e., charge), and interfacial adsorption.⁸ Many studies reporting enhanced rates of reaction have used an electrospray source to generate an aerosol plume.^{1–5} Electrospray sources produce highly charged and rapidly evaporating droplets, which could lead to increasing reactant concentrations, significant pH variability compared to the bulk (due to solvent oxidation by the charges in the droplets), and complex ion–ion and ion–solvent interactions. Further, the droplet plume exhibits a high surface area relative to the bulk volume, thus enhancing the role of interfacial adsorption in perturbing chemical kinetics.⁸ An increase in the surface to volume ratio of the droplets has been found to increase the reaction rate, suggesting the droplet surface could play a major role in the observed rate acceleration.⁷ Most measurements studying rate enhancements

in microdroplets use a polydisperse droplet source, which limits the control of both size distribution and time evolution of the reactant concentration.^{1–6} Microfluidic devices capable of generating a monodisperse droplet distribution have also been used to study rate enhancements in microdroplet emulsions.⁷ However, it remains unclear if the rate enhancing properties attributed to the oil–water interface of microfluidic devices are general to the air–water interface.

Another means of ensuring a monodisperse size is by limiting a study to a single droplet. The contactless confinement of single, micrometer-sized droplets has been established as a powerful method for probing the physical and chemical properties of liquids and heterogeneous interfaces.⁹ For example, aerosol optical tweezers (AOTs) have been used to measure the surface tension, viscosity, and hygroscopicity of a wide variety of aqueous samples, while electrodynamic balance (EDB) methods have allowed rapid mass transport and transformation processes to be interrogated.⁹ AOTs provide

Received: September 9, 2017

Accepted: October 19, 2017

Published: October 19, 2017

powerful, real-time characterization of droplets via the morphology dependent resonances that appear in the Raman spectrum of the droplet induced by the trapping laser. Also, a holographic optical trap (HOT) can manipulate arrays of droplets and bring selected droplets into contact when desired. All droplets confined in a HOT can be fully characterized using cavity enhanced Raman spectroscopy to determine their size to nanometer accuracy before they are mixed together.¹⁰ EDBs are extremely versatile techniques and offer advantages over AOT methods due to the facile introduction of single droplets into the confinement region and the ability to trap particles that strongly absorb laser light. EDBs can trap a larger range of droplet sizes than AOTs (from 100s nm¹¹ to 100 μm diameter for EDBs⁹ compared with <10 μm for AOTs¹⁰). A wide range of electrode configurations have been developed (e.g., double ring, cylindrical, and quadrupole) to facilitate a broad range of measurements, including the study of Mie scattering,¹² hygroscopicity and phase transitions,^{13,14} heterogeneous chemistry,^{15,16} ice nucleation,^{17–19} and mass transport from droplets.^{20,21} In these measurements, compositional changes in confined particles are typically the result of interfacial processes, such as mass transport (evaporation and/or condensation of semivolatile and volatile material) or chemical changes due to reactive gas uptake. This makes bulk initiated chemistry difficult to study in conventional EDB configurations because it is hard to initiate a reaction cleanly at a well-defined time in a single droplet with no external reactant source.

Optical probes, such as Raman spectroscopy, typically used to characterize droplets in an EDB or AOT are limited to functional group information and cannot provide information about the exact chemical composition of the droplet as it undergoes reactive transformations.⁹ As evident from previous rate enhancement measurements,^{1–6} mass spectrometry of droplets can provide quantitative chemical information, but studies characterizing single droplets with mass spectrometry are limited. Previously, free-falling droplets have been ionized directly by impaction on a highly charged needle, forming a spray that is directed toward a mass spectrometer.²² Several studies have performed mass spectrometry on single, levitated droplets in an acoustic trap (which uses ultrasonic waves to confine particles) coupled to a laser desorption^{23,24} or a direct analysis in real time (DART) ionization source.²⁵ However, because of the strong electric fields in EDBs and the small size of the trapped droplet, nondestructive mass spectrometry is difficult (i.e., particles need to be removed from the trap and ionized completely). Previous work has shown droplets can be ejected from a double ring electrode, deposited onto a matrix and ionized using matrix assisted laser desorption ionization.²⁶ However, the delay between deposition and detection is not ideal for real-time reaction monitoring, and direct ionization of droplets as they exit the EDB is preferred. Very recently, work has quantified evaporation from microdroplets by ejecting single droplets from a double ring electrode, vaporizing them on a heated platform, and ionizing the components using a corona discharge.²⁷

In order to further explore chemical transformations in micrometer-sized compartments, we present here a new EDB electrode arrangement—the branched quadrupole trap (BQT)—that is capable of merging confined droplets. Merged droplets have previously been trapped using a tandem electrodynamic trap and observed spectroscopically.²⁸ The BQT allows for rapid changes in composition via droplet coalescence (enabling the study of bulk initiated processes) and

allows for the ejection of single droplets into an ionization source for mass spectral analysis (enabling chemical characterization of droplets). By coupling droplet confinement techniques with high resolution mass spectrometry, it is possible to measure condensed phase chemical kinetics in microcompartments under well-defined conditions. Due to the droplet size range over which EDB methods operate (1–10s μm) and their ability to control droplet composition by changing environmental conditions, they represent a unique way to study chemical reactions in a potentially interesting droplet size regime. In this work, we characterize the mixing times of merged droplets and demonstrate the application of the technique to probing chemical processes in droplets using both fluorescence spectroscopy and single droplet paper spray (PS) mass spectrometry.

EXPERIMENTAL SECTION

Branched Quadrupole Trap Design. A linear quadrupole EDB allows arrays of droplets to be confined along the axis of four rods, as has been discussed previously.^{11,29} In order to facilitate merging of different droplet populations, the BQT design has been developed (shown in Figure 1). Aqueous

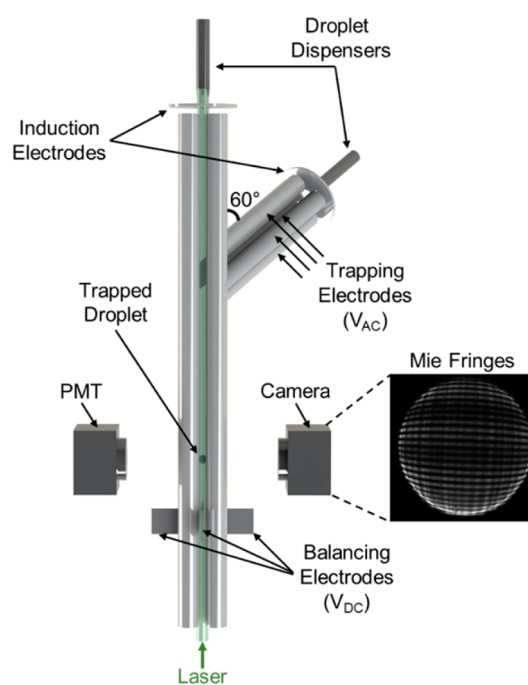


Figure 1. Schematic of the BQT. Different solutions necessary for a chemical reaction are dispensed from the two droplet dispensers. Thus, when the droplets from each of the dispensers coalesce, a chemical reaction in the merged, trapped droplet can be initiated. The chamber that houses the BQT setup and the optics used to collect and collimate the light for the camera and PMT are not shown. An example of the far field image of elastically scattered light used to determine the size of the trapped droplet is shown.

droplets are generated using a piezoelectric dispenser with a 50 μm orifice (Microfab, Inc.) and are introduced into the top of the BQT along the linear axis. During actuation of the dispenser, a high voltage (typically <1 kV) is applied to an induction electrode to induce a net charge on the droplet, allowing it to become confined within the electric field of the BQT. Droplets generally have a net charge on the order of

10^{-13} C ($\sim 10^6$ elementary charges),³⁰ which leads to surface charge densities that are ~ 100 times smaller than those found in electrospray droplets.³¹ The BQT consists of four stainless steel trapping electrodes arranged in a quadrupole configuration. An alternating voltage (V_{ac}) with an amplitude of 300–500 V and frequency of 200–400 Hz is applied to the trapping electrodes to confine the charged droplets axially along the rods.

A set of branching electrodes that extend off the linear trap at a 60° angle allow two separate droplet dispensers to be used concurrently or simultaneously. By using two different solutions in each of the dispensers, chemistry can be initiated when droplets from each of the dispensers collide. Droplets dispensed from both the vertical dispenser and branch dispenser travel ~ 12 cm before they enter the common, lower portion of the trap. Droplets are held in the lower trap using a set of balancing electrodes that consist of stainless steel blades extending symmetrically between the rods toward the center of the quadrupole trap. By applying a static voltage (up to ± 500 V) to these electrodes, the gravitational force acting on the droplet can be overcome, leading to contactless levitation of the droplet.

Once confined within the trap, droplets are illuminated with a 532 nm laser (Changchun New Industries Optoelectronic Tech.) introduced axially. Scattered light from the laser is collected (using an optical scheme that has been previously reported)³² and imaged in the far field with a CMOS camera (Thorlabs, Inc.) using a 532 nm line pass filter. The far field image serves two purposes: droplet positioning and sizing. A feedback loop controlling the voltage applied to the balancing electrodes is used to keep the droplet centered in the far field image and stationary in the trap. For example, as a droplet evaporates and loses mass, the magnitude of the voltage applied to hold the droplet decreases to keep the droplet fixed in space. Additionally, the far field image contains interference fringes from Mie scattering with distinct maxima and minima. The angular spacing of these fringes, the wavelength of scattered light (532 nm), and the refractive index of the droplet (1.36 for the ~ 3 M LiCl droplets)³³ are used with the geometrical optics approximation to determine the radius of the droplet.³⁴ An additional 355 nm laser (JDS Uniphase) is introduced coaxially with the 532 nm laser and is used to excite fluorescence in the confined droplet.

The BQT is housed within an environmentally controlled chamber, and most experiments were performed in a high relative humidity (RH $\sim 90\%$) atmosphere generated by passing $200\text{--}500$ cm³(STP) min⁻¹ of nitrogen gas through a water bubbler. The RH of the gas is measured with two separate RH sensors (Honeywell International, Inc.) located at the inlet and outlet of the chamber. The nitrogen flow exerts a downward force on the trapped droplets and facilitates droplet ejection into the mass spectrometer when the DC trapping voltage is removed.

Merging Droplets in the BQT. In a typical merging experiment, a single droplet is dispensed from the side arm dispenser and held in the lower trap. A second droplet from the vertical dispenser is generated and merges with the confined droplet. The voltages applied to the induction electrodes are set to produce droplets of opposite polarity (droplets with the same charge polarity will not merge). The initial droplet (from the side arm dispenser) has a larger net charge than that from the vertical dispenser. When droplets merge, there is a decrease in the overall charge and an increase in the mass of the droplet,

which both cause the merged droplet to fall lower in the trap. The initial position of the droplet is restored by increasing the voltage applied to the balancing electrodes using the voltage feedback loop. Droplet size is determined from the fringe separation from Mie scattering in the far field image both before and after merging the event. The change in radius with the merging event is used to infer the size of the merged droplet. As shown in Figure 2, the radii of the triggered and

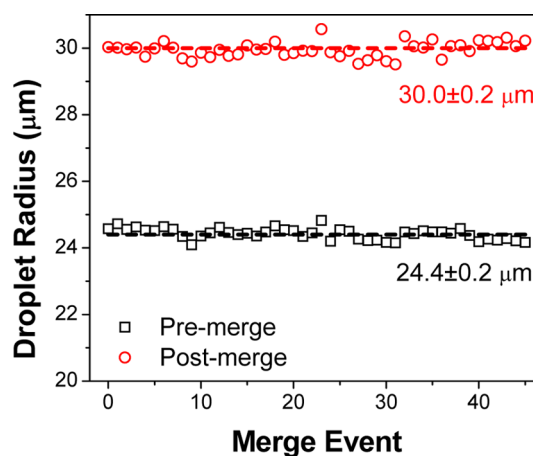


Figure 2. Measured droplet radius before and after merging for 45 separate coalescence events (~ 2 h of operation). Droplets contained ~ 3 M LiCl. The dashed lines show the average droplet radius.

merged droplets are very repeatable (± 200 nm, 0.7% relative standard deviation). The size of the held droplet is controlled by changing the water activity of the initial solution with a soluble salt ($\sim 0.4\text{--}6$ M LiCl) and allowing the droplet to equilibrate with the trap conditions. The size of the merging droplet is controlled by changing the shape (i.e., magnitude and duration) of the square wave electrical pulse used to generate the droplet with the piezoelectric microdispenser.³⁵ As the merging droplet diameter increases, its terminal velocity changes from 0.07 to 0.15 m/s for 39 and 55 μ m diameter droplets, respectively. Compared to previously reported droplet merging approaches in an EDB,²⁸ the BQT approach does not separate droplet coalescence from spectroscopic study. Thus, fast reactions (such as mixing dynamics in droplets) can easily be studied using the BQT.

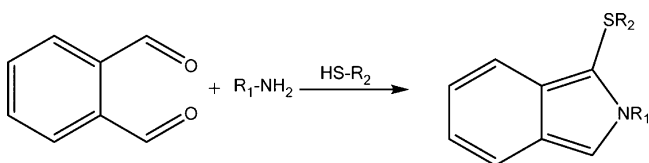
We have applied two different methods to study the merging process and the evolving chemical composition of droplets. Fluorescence emitted by the droplet is collected and focused onto a photomultiplier tube (PMT, Hamamatsu Photonics) using a plano-convex lens ($f/30$ mm). The fluorescence emitted by the droplet is used to quantify mixing times and reaction kinetics. A PS ionization source is used for single droplet mass spectrometry measurements to detect the products of a reaction.

Mixing Times from Droplet Fluorescence. The mixing time in a merged droplet is measured to determine the fastest reactions that can be studied using the BQT. This time is measured by quantifying the acid-induced quenching of rhodamine B (RhB), a fluorescent dye. Fluorescence from a droplet containing 500 μ M RhB and LiCl is excited using the 532 nm laser and detected with the PMT using a 550 nm long pass filter to remove any elastically scattered light. Fluorescence from the RhB droplet is quenched by merging it with a sulfuric acid droplet (2–20% (v/v)). The decay of fluorescence

intensity upon droplet coalescence is measured with the PMT (data acquisition rate = 500 kHz). Mixing is studied by (1) changing the size of the trapped droplet and keeping the size of the merging droplet constant; (2) keeping the size of the trapped droplet constant and changing the size of the merging droplet; and (3) changing the concentration of sulfuric acid in the merging droplet.

Reaction Kinetics from Droplet Fluorescence. Fluorescence is used to measure chemical kinetics in a single droplet which can be directly compared to those in the bulk solution. The chemical reaction between *o*-phthalaldehyde (OPA) and alanine in the presence of dithiothreitol (DTT) yields an isoindole product that fluoresces at ~ 400 – 500 nm (Scheme 1).^{36,37} Solutions of OPA and alanine are prepared in a 3 M

Scheme 1. Reaction of *o*-Phthalaldehyde (OPA) with a Primary Amine (Alanine) in the Presence of a Thiol Group (Dithiothreitol, DTT) Yielding a Fluorescent Isoindole Compound



LiCl solution that is buffered with a 50 mM borate buffer (pH = 9). Alanine solutions have concentrations of 5.3, 10.3, 15.3, 20.8, and 33.3 mM. OPA and DTT are mixed together (to form a stable adduct)³⁷ and have concentrations of 5.3 mM and 7.8 mM, respectively. Fluorescence from merged alanine and OPA droplets is excited by the 355 nm laser and measured with the PMT using a 450 ± 20 nm bandpass filter to remove elastically scattered laser light. At least 10 trials are used for each reaction condition in the droplets. Reaction kinetics measured in droplets are compared to those measured in the bulk as described in the Supporting Information.

Single Droplet Paper Spray Mass Spectrometry. By coupling a PS ionization source to the exit of the BQT, we have developed a new approach to determine how the chemical composition of a single droplet changes over the course of a reaction. A schematic of the experimental setup is shown in Figure 3a. The details of PS mass spectrometry and its applications have been previously described.^{38,39} Here, a PS ionization source is generated by cutting a small triangle (~ 6 mm base, ~ 10 mm height) from chromatography paper (Whatman 3MM), passing a solvent through it, and applying a 4–5 kV potential. The tip of the PS is placed ~ 2.5 cm from the inlet of the mass spectrometer (Q-Exactive Orbitrap, Thermo Fisher Scientific, Inc.). The large electric field at the tip of the paper causes a spray to form that is directed toward the mass spectrometer. A 0.8–1.0 mL/h flow of 1% formic acid solution in methanol through the filter paper maintains continuous operation of the PS source. The mass spectrometer is operated with a resolution of 17,500 and a maximum ion injection time of 50 ms.

A 2 cm long piece of 1/4 in. stainless steel tubing is affixed to the exit of the BQT coaxial with the trap. The BQT is positioned such that the exit of this tubing is ~ 1 cm above the tip of the PS source. After merging, droplets are held in the trap for a fixed period of time. Following a delay, the voltage applied to the balancing electrodes is removed and the droplet falls from the trap (typically aided by the flow of humidified

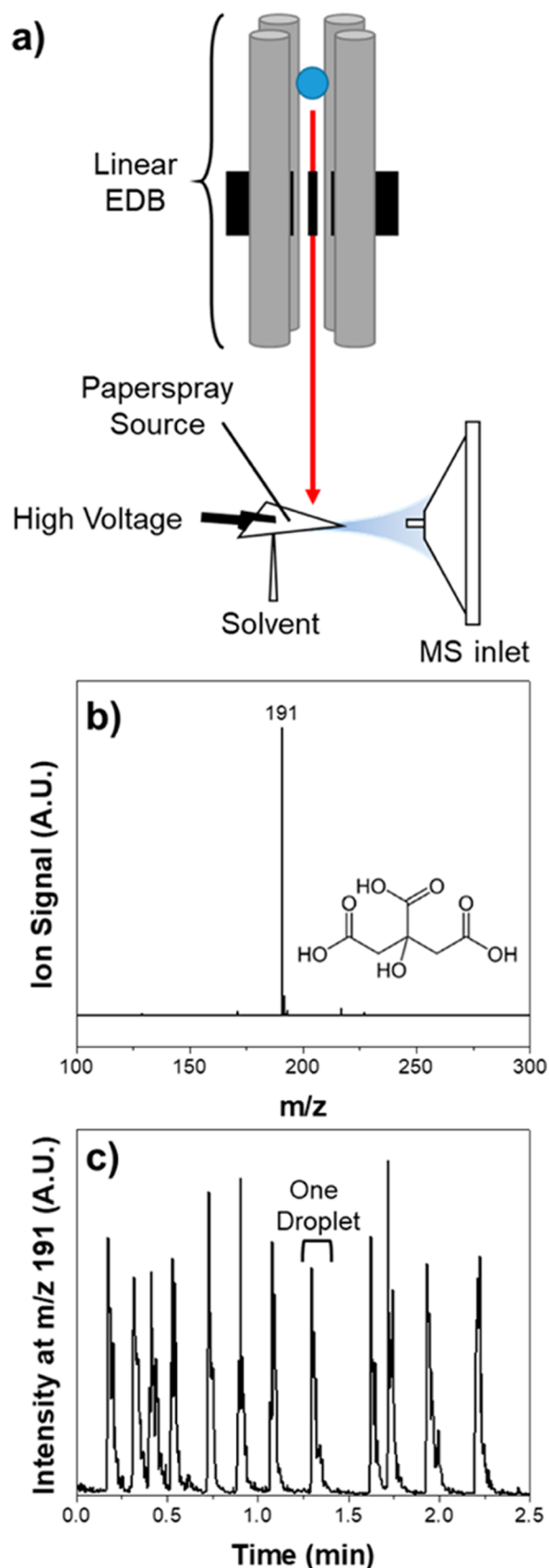


Figure 3. (a) Schematic of the BQT/PS mass spectrometry interface. (b) Mass spectrum from a single $50 \mu\text{m}$ diameter, 0.2% (w/v) citric acid droplet. (c) Selected ion chromatogram of citric acid droplets. Each spike in the chromatogram represents one $50 \mu\text{m}$, 0.2% citric acid droplet impacting the PS source.

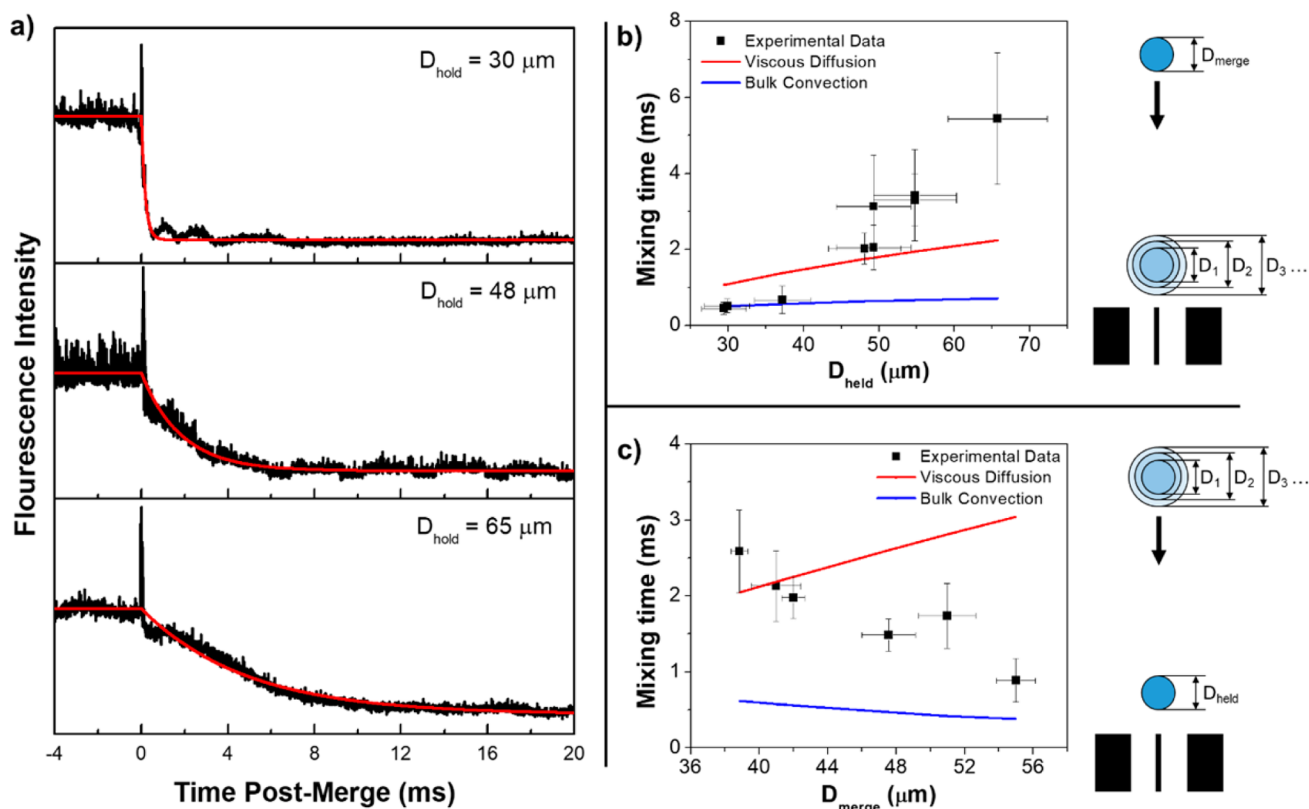


Figure 4. (a) Fluorescent quenching of differently sized RhB droplets with the coalescence of a $38 \pm 3 \mu\text{m}$, 20% (v/v) sulfuric acid droplet. The fluorescence intensity measured with the PMT (black line) is fit to eq 1 to extract a mixing time. The fit to the data is shown by the red line. The data shown have mixing times of 0.191 ± 0.006 , 1.82 ± 0.03 , and 4.93 ± 0.06 ms for the 20, 48, and $65 \mu\text{m}$ RhB droplets, respectively. (b) Mixing times for experiments where the merging droplet diameter (sulfuric acid) is kept constant ($38 \pm 3 \mu\text{m}$) and the held droplet diameter (RhB) is varied. The viscous diffusion and bulk convection times are shown in red and blue, respectively. The molecular diffusion times are too long to show on this scale. The experimental mixing times scale with the volume of the held droplet. (c) Mixing times for experiments where the merging droplet diameter (sulfuric acid) is increased and the held droplet diameter (RhB) is kept constant ($56 \pm 2 \mu\text{m}$). As the diameter of the merging droplet increases, the mixing time decreases.

nitrogen), impinging on the tip of the PS source. The flow of solvent dilutes the droplets and pushes the components in the droplet toward the tip of the filter paper where they are ionized and sprayed into the mass spectrometer. Compared to electrospray techniques with droplets,⁴⁰ the PS source slows down the ionization event and ensures the entire droplet is sampled. Figure 3b shows a mass spectrum that is collected from a single, $50 \mu\text{m}$ diameter droplet of 0.2% citric acid (~ 0.6 ng of citric acid total). Due to its low vapor pressure and previous use in our laboratory,⁴¹ citric acid is used to benchmark the sensitivity and reproducibility of the single droplet PS mass spectrometry technique. The mass spectrometer is operated in negative mode, and the only peak observed is from deprotonated citric acid ($[M - H]^-$) at m/z 191. Figure 3c shows the time profile of the peak at m/z 191. Each individual spike arises from the impact of one droplet on the PS source. The average peak area of these droplets has a relative standard deviation of $\sim 15\%$ (likely due to variation in where the droplet impacts the PS source). The precision of this method could be improved with the use of an internal standard in the droplet.

The products of the reaction between OPA and alanine in the absence of LiCl are studied using single droplet PS mass spectrometry. Because the large amount of LiCl that is used in the fluorescence experiments significantly diminishes the ionization efficiency of the organic species by the PS source,

LiCl is not added for the single droplet mass spectrometry experiments. Solutions of 10.7 mM OPA with 21.4 mM DTT and 30.0 mM alanine are prepared in a 50 mM borate buffer (pH ~ 9). The mass spectrometer is operated in positive ion mode to study both the components of pure, unreacted OPA and alanine droplets as well as merged, reacted droplets.

RESULTS AND DISCUSSION

In order to facilitate an understanding of the observed reaction kinetics, we first describe the mixing times that are observed in merged droplets and the experimental parameters that control them. Then, both kinetic and product analyses of the reaction between OPA and alanine in droplets are presented. Reaction kinetics measured with fluorescence imaging are reported in [Chemical Reactions in Merged Droplets](#). The OPA/alanine reaction products that were observed with single droplet PS mass spectrometry are presented in [Single Droplet Mass Spectrometry](#).

Mixing Times in Merged Droplets. The fastest reaction kinetics that can be measured in a well-mixed droplet following coalescence is dependent on the time scale for mixing in the merged droplets. Here, the time it takes for a merged droplet to mix completely is measured by quantifying the quenching rate of a fluorescent dye. RhB fluorescence is quenched by a change in pH of solution; at low pH fluorescence is quenched almost entirely (Figure S-1, [Supporting Information](#)). Figure 4a shows

examples of how the fluorescence from differently sized RhB droplets (500 μM) is quenched when they merge with 20% (v/v) sulfuric acid droplets of a constant diameter ($38 \pm 3 \mu\text{m}$). The initial rise in fluorescence intensity is due to the increase in the cross-sectional area of the droplet illuminated by the laser. As the coalesced droplet relaxes from initially dumbbell-shaped to spherical, its cross-sectional area changes, causing the observed fluorescence intensity to oscillate. A similar effect is observed (and has been reported previously⁴²) in elastically scattered light (Figure S-2, Supporting Information). The angular frequency and damping of this oscillation is related to the surface tension and viscosity of the merged droplet, respectively.⁴² Droplets typically relax to a spherical shape after $\sim 200 \mu\text{s}$. The fluorescence transients are fit to the following piecewise exponential decay function to extract mixing times:

$$I = \begin{cases} a + b, & t < c \\ ae^{-(t-c)/d} + b, & t \geq c \end{cases} \quad (1)$$

where a is the quenched fluorescence intensity, b is the fluorescence intensity postquenching, c is the time delay between data collection and droplet merging, and d is the mixing time. The red lines shown in Figure 4a are the fits of eq 1 to the fluorescence transients. Because the lifetimes of surface oscillations are typically shorter than the observed mixing times and their magnitude is less than the change due to quenching, surface oscillations are not explicitly considered in eq 1.

To better understand the observed mixing times, they are compared to the time scales for molecular diffusion, viscous diffusion, and bulk convection. The characteristic time for molecular diffusion (τ_{diff}) is

$$\tau_{\text{diff}} \sim \frac{L_{\text{ch}}^2}{D} \quad (2)$$

This is the time needed for a molecule to diffuse one characteristic length (L_{ch}) in a fluid with mass diffusivity D . For RhB in water, D is $4.2 \pm 0.3 \times 10^{-10} \text{ m}^2 \text{ s}^{-1}$.⁴³ L_{ch} for the merged droplet is calculated from the held (D_{held}) and merging (D_{merge}) droplet diameters as follows:⁴⁴

$$L_{\text{ch}} = \frac{2D_{\text{held}}D_{\text{merge}}}{D_{\text{held}} + D_{\text{merge}}} \quad (3)$$

For the droplet conditions here, molecular diffusion time is typically $\sim 1\text{--}10 \text{ s}$.

The viscous diffusion time scale (τ_{visc})—which represents the time required for momentum to diffuse one characteristic length scale in a fluid with kinematic viscosity ν —is

$$\tau_{\text{visc}} \sim \frac{L_{\text{ch}}^2}{\nu} \quad (4)$$

For an $\sim 3 \text{ M}$ LiCl solution, ν is $1.4 \times 10^{-6} \text{ m}^2 \text{ s}^{-1}$.⁴⁵ For the droplet conditions here, viscous diffusion is typically $1\text{--}10 \text{ ms}$.

Finally, the bulk convection time scale (τ_{conv}) is the time required for material to traverse one characteristic length at a rate equal to the relative droplet velocity (U_{rel}):

$$\tau_{\text{conv}} \sim \frac{L_{\text{ch}}}{U_{\text{rel}}} \quad (5)$$

The relative velocity of the collision is calculated from the terminal velocity of the merging droplet ($0.07\text{--}0.15 \text{ m/s}$). As the merging droplet approaches the balancing electrode, its

velocity increases slightly due to Coulombic attraction. However, based on the voltage applied to the balancing electrode, this acceleration is measured to be small (Supporting Information, Figure S-3). For droplets here, the bulk convection time is typically $\sim 200\text{--}600 \mu\text{s}$. Carroll and Hidrovo previously demonstrated that as the inertia of the collision event increases, the observed mixing times are shortened toward the bulk convection time scale.⁴⁴

Figure 4b shows the measured mixing times when the size of the held droplet is changed and the diameter of the merging droplet is held constant ($D_{\text{merge}} = 38 \pm 3 \mu\text{m}$). As the size of the held droplet decreases, the observed mixing time decreases toward the convection mixing time. A log–log plot of initial droplet diameter vs mixing time has a slope of 3.2 ± 0.2 (Figure S-4, Supporting Information), implying that the mixing rate in this experiment scales with the volume of the held droplet.

Figure 4c shows the mixing times when the size of the held droplet is constant ($D_{\text{held}} = 56 \pm 2 \mu\text{m}$), and the diameter of the merging droplet is changed. As the diameter of the merging droplet increases, the diameter of the merged droplet increases (which causes the viscous diffusion time to increase) and the terminal velocity of the merging droplet increases (which causes the bulk convection time to decrease). The experimental data show that mixing times decrease with increasing merging diameter. This is likely due to the increasing energy and inertia of the collision.⁴⁴ If the inertia of the collision were to continue to increase, the mixing time is predicted to follow the bulk convection time.⁴⁴ Finally, when the concentration of sulfuric acid is changed (and the held/merging droplet diameters are kept constant), the mixing times do not change (Figure S-5, Supporting Information). This suggests that the observed mixing times are controlled by the size of droplets and velocity of collisions and are not due to the concentration of reagents in the droplets.

The observed mixing times reported here (reliably down to $\sim 400 \mu\text{s}$) are very similar to those reported in free-droplet collision experiments (i.e., colliding droplets not confined within an electrodynamic balance).⁴⁶ They are also similar to those observed in conventional stopped flow kinetics measurements ($\sim 2 \text{ ms}$),⁴⁷ but slower than those achieved in miniaturized continuous flow methods such as theta capillary electrospray (mixing time $\sim 1 \mu\text{s}$)⁴⁸ and microfluidic channels (mixing time $\sim 15 \mu\text{s}$).⁴⁷ Work by Lee et al. colliding a plume of high speed (80 m/s) $13 \mu\text{m}$ droplets reports mixing times of a couple of microseconds.⁶ The mixing times in the BQT allow for the study of reactions with a bimolecular rate constant of up to $\sim 10^4\text{--}10^5 \text{ M}^{-1} \text{ s}^{-1}$. As shown, faster mixing times could be achieved by either using smaller droplets or increasing the velocity of the collision. The latter could be accomplished either electrostatically (e.g., apply a higher potential to the balancing electrodes, Figure S-3) or with a faster flow of gas through the trap.

Chemical Reactions in Merged Droplets. The reaction between OPA and alanine in the presence of DTT (Scheme 1) is studied in droplets with the BQT and bulk solution using fluorescence spectroscopy. LiCl is added to the solutions to decrease the water activity such that evaporation from the droplet is minimized and the conditions in the droplet can be reproduced in the bulk. Because the water activity of a 3.0 M LiCl solution is 0.87 ,⁴⁹ experiments are performed with a RH close to 87% , and the size of the droplet does not change considerably over the time of the experiment (Figure S-6, Supporting Information). In bulk measurements, the volumes

of the reactant solutions are mixed in a 1:1 ratio, and the initial reactant concentrations are half the value of the prepared solutions. In droplets, the initial reactant concentrations are determined using the size of the merging droplets ($24.3 \pm 0.2 \mu\text{m}$ and $23.0 \pm 0.6 \mu\text{m}$ radii for alanine and OPA, respectively). The merged droplet has a radius of $29.9 \pm 0.4 \mu\text{m}$. While keeping the initial OPA concentration constant ($\sim 2.6 \text{ mM}$), the rate of fluorescence appearance is measured at various alanine concentrations ($\sim 2.6, 5.2, 7.7, 10.4,$ and 16.7 mM). Figure 5 shows an example of the bulk and droplet fluorescence

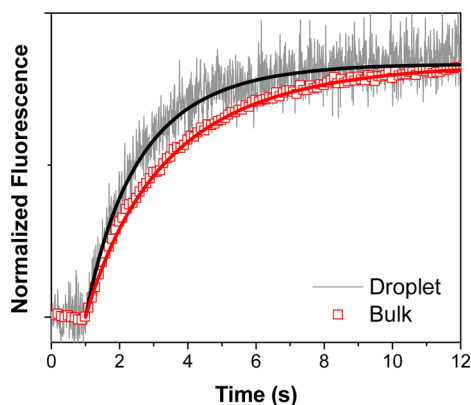


Figure 5. Fluorescence ($450 \pm 20 \text{ nm}$) generated from the reaction of OPA with alanine in a droplet with a radius of $29.9 \pm 0.4 \mu\text{m}$ (gray line) and in bulk solution (red squares). In the droplet, the initial OPA concentration is $2.4 \pm 0.1 \text{ mM}$ and the initial alanine concentration is $8.1 \pm 0.4 \text{ mM}$. In bulk solution, the initial concentration of OPA is 2.6 mM and the initial concentration of alanine is 7.7 mM . The solid black and red lines are the best-fit product concentrations from the bimolecular reaction simulation. The average bimolecular rate constant for the reaction of alanine with OPA is found to be 84 ± 10 and $67 \pm 6 \text{ M}^{-1} \text{ s}^{-1}$ in the droplet and bulk, respectively. The individual rate constants for the different reaction conditions are tabulated in Table S-1.

data that are collected with ~ 2.6 and $\sim 7.7 \text{ mM}$ initial OPA and alanine concentrations, respectively. Fluorescent intensity in the droplet appears at a slightly faster rate than in the bulk solution. To quantify the reaction rate constants in the merged droplet and bulk, the OPA and alanine reaction is simulated and fit to experimental data.

When the alanine concentration exceeds the OPA concentration, the final fluorescence intensity does not change with increasing amounts of alanine. At these conditions, it is assumed that the final concentration of the fluorescent product is equal to that of the initial OPA concentration. Using this scaling, the measured fluorescence intensity is converted to the concentration of fluorescent product. The reaction between OPA and alanine has previously been shown to follow bimolecular kinetics.³⁶ Thus, to quantify the rate of reaction in bulk and droplets, an ordinary differential equations solver is used to simulate a bimolecular reaction with the initial reactant concentrations set to experimental values. The bimolecular rate constant in the simulation is varied to best match the simulated and experimental product concentrations. The same kinetic analysis is used for both bulk and droplet experiments. The solid lines in Figure 5 represent the simulated product concentrations with the optimized rate constant. The average bimolecular reaction rate constants in the bulk and droplet are 67 ± 6 and $84 \pm 10 \text{ M}^{-1} \text{ s}^{-1}$, respectively. Uncertainty

corresponds to the standard deviation of the rate constants extracted at each reaction condition. The simulated fits and individual rate constants extracted at each reactant condition are tabulated in the Supporting Information (Figure S-7 and Table S-1). The bimolecular rate constant for the reaction of alanine with OPA in the presence of DTT has previously been measured to be $60 \pm 4 \text{ M}^{-1} \text{ s}^{-1}$,³⁶ which is in good agreement with the bulk rate constant reported here.

The average rate constant in the $30 \mu\text{m}$ radius droplet is roughly 25% larger than the rate constant in the bulk. When the polarity of the charge on the droplet is reversed (i.e., the merged droplet has a net positive charge instead of net negative charge), the kinetics of the reaction are unchanged (Figure S-8 in the Supporting Information). This suggests that the small amount of charge on the droplet surface does not affect the overall rate of reaction. Because evaporation from the particle is minimized with the addition of LiCl, the small observed rate enhancement could originate from enhanced surface to volume ratio in the droplet compared to the bulk. Fallah-Araghi et al. previously measured the kinetics of a bimolecular reaction in aqueous droplets in an oil–water emulsion. They observed a maximum rate enhancement by a factor of ~ 40 that decreased with increasing droplet radius. The observed enhancement was attributed to the increasing surface to volume ratio at smaller droplet sizes. A weak adsorption of molecular species to the oil–water interface was predicted to change the energetics of the reaction to favor product formation. However, a rate enhancement was only observed in emulsions that had a radius smaller than $\sim 20 \mu\text{m}$.⁷ The merged droplets in this study have a radius of $29.4 \pm 0.4 \mu\text{m}$, which could indicate that the droplets used here are still too large to observe a significant rate enhancement from interfacial effects.

Single Droplet Mass Spectrometry. The products of the reaction between OPA and alanine are studied using the PS ionization source. Figure 6a shows mass spectra from a single alanine droplet (black line) and OPA solution droplet (red line). Compared to the concurrently developed single droplet mass spectrometry method (which uses a corona discharge to ionize the vaporized droplet components),²⁷ the use of the PS ionization source leads to less fragmentation and easier identification of reaction products. The alanine spectrum has only one peak at m/z 90, which represents the protonated molecular ion. The OPA spectrum has peaks at m/z 135 and 157, which are from the protonated OPA molecule and the OPA/ Na^+ complex, respectively. The peak at m/z 311 corresponds to the OPA and DTT adduct complexed with a Na^+ ion. OPA reacts with thiol-containing compounds to create a stable 1,3-dihydroisobenzofuran compound that has been previously observed.³⁷ Because DTT has two reactive thiol groups, a single DTT molecule can react with two OPA molecules. The peak at m/z 445 corresponds to this reaction product complexed with a Na^+ ion. Figure 6a also shows the mass spectrum of a single merged droplet after it has reacted for 6 s (blue line). Because alanine is in excess in the merged droplet, only the intensities of the peaks from OPA-containing species have decreased significantly (the alanine peak remains a dominant peak). The peaks present at m/z 342 and 476 correspond to the protonated isoindole reaction products.^{36,37} The chemical structures for each of the ions are shown in the Supporting Information (Table S-2).

Figure 6b shows a selected ion chromatogram from the ejected merged droplets for each of the peaks of interest in the experiment (m/z 90, 311, 342, 445, and 476). All of the ions

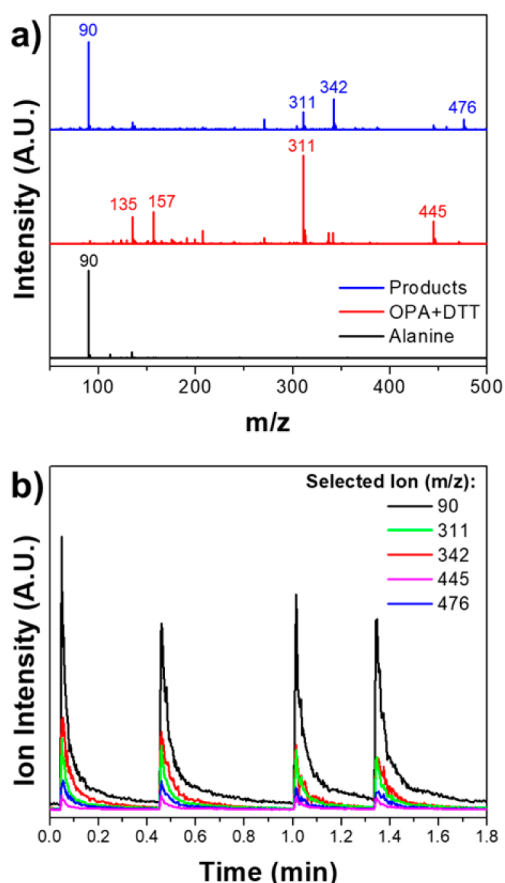


Figure 6. (a) Mass spectra of single droplets from alanine solution (black line), OPA/DTT solution (red line), and merged alanine/OPA droplets after 6 s of reaction (blue line). The new peaks in the products spectrum (m/z 342 and 476) correspond to the expected fluorescent products. The chemical structures of labeled peaks are given in the Supporting Information (Table S1). (b) Selected ion chromatograms showing the time response of each peak of interest in the merged droplets. The signal-to-noise ratio for each of these peaks is >100 .

show a similar time response and are only present when a droplet is ejected onto the PS source. A ~ 5 mM aqueous droplet with a radius of $30 \mu\text{m}$ (similar to the OPA conditions in this experiment) has ~ 0.5 pmol of material (<1 ng). As shown in Figure 6b, this results in single droplet pulses with a signal-to-noise (S/N) ratio > 100 . Assuming a S/N ratio of ~ 10 is necessary to quantify peak intensities, a single, ~ 5 mM droplet with a radius of $\sim 15 \mu\text{m}$ could easily be detected in the current configuration.

CONCLUSION

A branched quadrupole trap has been designed and constructed to merge confined droplets. This trap allows for new measurements of homogeneous chemical reactions in droplets. Through the quenching of fluorescence of RhB droplets by sulfuric acid droplets, consistent mixing times as short as $\sim 400 \mu\text{s}$ are obtainable using droplets moving at relative velocities of ~ 0.1 m/s. As predicted by Carroll and Hidrovo,⁴⁴ mixing experiments in the BQT show that faster mixing times are achievable by either decreasing the size of the merging droplets or increasing the speed of the collision. With these mixing times, chemical reactions with a bimolecular rate constant up to

$\sim 10^4$ – $10^5 \text{ M}^{-1} \text{ s}^{-1}$ can be studied in the BQT in its current form.

The ability to measure homogeneous chemical reactions in the BQT has been demonstrated using both fluorescence spectroscopy and single droplet PS mass spectrometry. The reaction of OPA with alanine (in the presence of DTT) is found to occur slightly faster ($\sim 25\%$) in a droplet with a radius of $\sim 30 \mu\text{m}$ than in bulk solution. Charge on the droplet and changes in the concentration of reactants due to evaporation do not play a significant role in any potential rate enhancement in the fluorescence experiments reported here. Thus, the small rate enhancement is attributed to the larger surface to volume ratio of the droplet compared to the bulk. Single droplet PS mass spectra of reacted droplets following merging show the expected reaction products. Based on the observed signal levels, it is estimated that single droplets with a radius of $\sim 15 \mu\text{m}$ with <100 pg of analyte could be easily detected using PS mass spectrometry.

We have developed a new technique for the contactless manipulation and merging of micrometer-sized droplets to initiate chemistry. We demonstrate the applicability of fluorescence imaging for measuring reaction kinetics and demonstrate the use of mass spectrometry coupled with a single particle trap. Going forward, these developments will allow for rigorous probing of reaction kinetics in a variety of samples spanning a wide range of sizes and concentrations.

ASSOCIATED CONTENT

Supporting Information

The Supporting Information is available free of charge on the ACS Publications website at DOI: 10.1021/acs.analchem.7b03704.

Measurement details, fluorescence spectra, scattered light intensity results, images of droplets, mixing time vs held droplet diameter log–log plot, mixing time as function of acid concentration, droplet radius changes over time, product concentrations with different conditions, reaction of OPA and alanine in charged trapped droplets, rate constants, and chemical structures (PDF)

AUTHOR INFORMATION

Corresponding Author

*E-mail: krwilson@lbl.gov. Tel.: (510) 495-2474.

ORCID

Michael I. Jacobs: 0000-0003-3682-0409

Ryan D. Davis: 0000-0002-4434-1320

Frances Houle: 0000-0001-5571-2548

Kevin R. Wilson: 0000-0003-0264-0872

Present Address

[§]Stanford Linear Accelerator Center, Menlo Park, CA 94025, USA.

Notes

The authors declare no competing financial interest.

ACKNOWLEDGMENTS

Early work on the design and construction of the BQT was supported by an Early Career Award (K.R.W. and J.F.D.) from the Condensed Phase and Interfacial Molecular Science Program, in the Chemical Sciences Geosciences and Biosciences Division of the Office of Basic Energy Sciences of the U.S. Department of Energy under Contract No. DE-AC02-

05SCH11231. The portion of this work on mixing time scales is supported by the Laboratory Directed Research and Development (LDRD) program at Lawrence Berkeley National Laboratory. M.I.J. is supported by a NSF Graduate Research Fellowship under DGE-1106400.

REFERENCES

- (1) Bain, R. M.; Pulliam, C. J.; Cooks, R. G. *Chem. Sci.* **2015**, *6* (1), 397–401.
- (2) Girod, M.; Moyano, E.; Campbell, D. I.; Cooks, R. G. *Chem. Sci.* **2011**, *2* (3), 501.
- (3) Banerjee, S.; Prakash, H.; Mazumdar, S. *J. Am. Soc. Mass Spectrom.* **2011**, *22* (10), 1707–1717.
- (4) Müller, T.; Badu-Tawiah, A.; Cooks, R. G. *Angew. Chem., Int. Ed.* **2012**, *51* (47), 11832–11835.
- (5) Banerjee, S.; Zare, R. N. *Angew. Chem., Int. Ed.* **2015**, *54* (49), 14795–14799.
- (6) Lee, J. K.; Kim, S.; Nam, H. G.; Zare, R. N. *Proc. Natl. Acad. Sci. U. S. A.* **2015**, *112* (13), 3898–3903.
- (7) Fallah-Araghi, A.; Meguellati, K.; Baret, J.-C.; Harrak, A. E.; Mangeat, T.; Karplus, M.; Ladame, S.; Marques, C. M.; Griffiths, A. D. *Phys. Rev. Lett.* **2014**, *112* (2), 28301.
- (8) Yan, X.; Bain, R. M.; Cooks, R. G. *Angew. Chem., Int. Ed.* **2016**, *55* (42), 12960–12972.
- (9) Krieger, U. K.; Marcolli, C.; Reid, J. P. *Chem. Soc. Rev.* **2012**, *41* (19), 6631–6662.
- (10) Power, R. M.; Reid, J. P. *Rep. Prog. Phys.* **2014**, *77* (7), 074601.
- (11) Woźniak, M.; Derkachov, G.; Kolwas, K.; Archer, J.; Wojciechowski, T.; Jakubczyk, D.; Kolwas, m. *Langmuir* **2015**, *31*, 7860–7868.
- (12) Blau, H. H.; McCleese, D. J.; Watson, D. *Appl. Opt.* **1970**, *9* (11), 2522–2528.
- (13) Tang, I. N.; Munkelwitz, H. R. *J. Geophys. Res.* **1994**, *99*, 18801–18808.
- (14) Choi, M. Y.; Chan, C. K. *Environ. Sci. Technol.* **2002**, *36* (11), 2422–2428.
- (15) Lee, A. K. Y.; Chan, C. K. *Atmos. Environ.* **2007**, *41* (22), 4611–4621.
- (16) Pope, F. D.; Gallimore, P. J.; Fuller, S. J.; Cox, R. A.; Kalberer, M. *Environ. Sci. Technol.* **2010**, *44* (17), 6656–6660.
- (17) Krieger, U. K.; Colberg, C. A.; Weers, U.; Koop, T.; Peter, Th. *Geophys. Res. Lett.* **2000**, *27* (14), 2097–2100.
- (18) Svensson, E. A.; Delval, C.; Von Hessberg, P.; Johnson, M. S.; Pettersson, J. B. C. *Atmos. Chem. Phys.* **2009**, *9* (13), 4295–4300.
- (19) Hoffmann, N.; Kiselev, A.; Rzesanke, D.; Duft, D.; Leisner, T. *Atmos. Meas. Tech.* **2013**, *6* (9), 2373–2382.
- (20) Davies, J. F.; Miles, R. E. H.; Haddrell, A. E.; Reid, J. P. *Proc. Natl. Acad. Sci. U. S. A.* **2013**, *110* (22), 8807–8812.
- (21) Davies, J. F.; Haddrell, A. E.; Miles, R. E. H.; Bull, C. R.; Reid, J. P. *J. Phys. Chem. A* **2012**, *116* (45), 10987–10998.
- (22) Tracey, P. J.; Vaughn, B. S.; Roberts, B. J.; Poad, B. L. J.; Trevitt, A. J. *Anal. Chem.* **2014**, *86*, 2895–2899.
- (23) Westphall, M. S.; Jorabchi, K.; Smith, L. M. *Anal. Chem.* **2008**, *80* (15), 5847–5853.
- (24) Warschat, C.; Stindt, A.; Panne, U.; Riedel, J. *Anal. Chem.* **2015**, *87* (16), 8323–8327.
- (25) Crawford, E. A.; Esen, C.; Volmer, D. A. *Anal. Chem.* **2016**, *88* (17), 8396–8403.
- (26) Bogan, M. J.; Agnes, G. R. *Anal. Chem.* **2002**, *74* (3), 489–496.
- (27) Birdsall, A. W.; Krieger, U. K.; Keutsch, F. N. *Atmos. Meas. Technol. Discuss.* **2017**, in review, DOI: [10.5194/amt-2017-341](https://doi.org/10.5194/amt-2017-341)
- (28) Kohno, J. Y.; Higashiura, T.; Eguchi, T.; Miura, S.; Ogawa, M. *J. Phys. Chem. B* **2016**, *120* (31), 7696–7703.
- (29) Hart, M. B.; Sivaprakasam, V.; Eversole, J. D.; Johnson, L. J.; Czege, J. *Appl. Opt.* **2015**, *54* (31), F174–F181.
- (30) Haddrell, A. E.; Davies, J. F.; Yabushita, A.; Reid, J. P. *J. Phys. Chem. A* **2012**, *116* (40), 9941–9953.
- (31) Wilm, M. *Mol. Cell. Proteomics* **2011**, *10* (7), M111.009407.
- (32) Davies, J. F.; Haddrell, A. E.; Reid, J. P. *Aerosol Sci. Technol.* **2012**, *46* (6), 666–677.
- (33) Gao, D.; Guo, Y.; Yu, X.; Wang, S.; Deng, T. J. *Chem. Eng. Data* **2015**, *60* (9), 2594–2599.
- (34) Glantschnig, W. J.; Chen, S.-H. *Appl. Opt.* **1981**, *20* (14), 2499–2509.
- (35) Vaughn, B.; Tracey, P.; Trevitt, A. *RSC Adv.* **2016**, *6*, 60215–60222.
- (36) Trepman, E.; Chen, R. F. *Arch. Biochem. Biophys.* **1980**, *204* (2), 524–532.
- (37) Zuman, P. *Chem. Rev.* **2004**, *104* (7), 3217–3238.
- (38) Wang, H.; Liu, J.; Cooks, G. R.; Ouyang, Z. *Angew. Chem., Int. Ed.* **2010**, *49* (5), 877–880.
- (39) Lin, C. H.; Liao, W. C.; Chen, H. K.; Kuo, T. Y. *Bioanalysis* **2014**, *6* (2), 199–208.
- (40) Dong, J.; Rezenom, Y. H.; Murray, K. K. *Rapid Commun. Mass Spectrom.* **2007**, *21*, 3995–4000.
- (41) Davies, J. F.; Wilson, K. R. *Chem. Sci.* **2015**, *6* (12), 7020–7027.
- (42) Bzdek, B. R.; Power, R. M.; Simpson, S. H.; Reid, J. P.; Royall, C. P. *Chem. Sci.* **2016**, *7*, 274–285.
- (43) Gendron, P. O.; Avaltroni, F.; Wilkinson, K. J. *J. Fluoresc.* **2008**, *18* (6), 1093–1101.
- (44) Carroll, B.; Hidrovo, C. *Heat Transfer Eng.* **2013**, *34* (2–3), 120–130.
- (45) Ostroff, A. G.; Snowden, B. S., Jr.; Woessner, D. E. *J. Phys. Chem.* **1969**, *73*, 2784–2785.
- (46) Takano, Y.; Kikkawa, S.; Suzuki, T.; Kohno, J. Y. *J. Phys. Chem. B* **2015**, *119* (23), 7062–7067.
- (47) Shastry, M. C. C.; Luck, S. D.; Roder, H. *Biophys. J.* **1998**, *74* (5), 2714–2721.
- (48) Mortensen, D. N.; Williams, E. R. *Anal. Chem.* **2015**, *87* (2), 1281–1287.
- (49) Robinson, R. A. *Trans. Faraday Soc.* **1945**, *41*, 756–758.